

# Sub-mesoscale lateral density structure in the oceanic surface mixed layer

Phil Hosegood,<sup>1</sup> Michael C. Gregg,<sup>1</sup> and Matthew H. Alford<sup>1</sup>

Received 3 May 2006; revised 9 August 2006; accepted 18 October 2006; published 23 November 2006.

[1] We investigate the horizontal scales of density variability in the surface mixed layer (SML) in the North Pacific Subtropical Front (STF) during a period of highly variable atmospheric forcing. Wavelet analysis shows that horizontal density variability is not restricted to scales,  $L$ ,  $\geq 10$  km as previously suggested but extends to  $L = 2$  km. The limiting  $L$  varies strongly with location and corresponds to a local internal Rossby radius that accounts for transient stratification above the seasonal thermocline. Density compensation in the SML, achieved when temperature and salinity effects cancel in their effect on density, occurs at  $30^{\circ}\text{N}$  at the climatological front associated with the northern boundary of the STF where large thermohaline gradients are observed. At  $28^{\circ}\text{N}$ , however, temperature gradients within the SML are not compensated by salinity, and horizontal density gradients result in  $2 \leq L \leq 10$  km. Our observations suggest dynamic processes restratify the SML at scales rarely resolved by numerical models of the SML. Citation: Hosegood, P., M. C. Gregg, and M. H. Alford (2006), Sub-mesoscale lateral density structure in the oceanic surface mixed layer, *Geophys. Res. Lett.*, 33, L22604, doi:10.1029/2006GL026797.

## 1. Introduction

[2] The oceanic surface mixed layer (SML), the uppermost region of the ocean that is approximately homogenous in density, is maintained by buoyancy fluxes through the ocean surface, internal mixing and mechanical mixing by the wind. The SML is usually studied within the context of its vertical structure, as stratification inhibits vertical fluxes to the main thermocline where they can influence the ocean interior. Understanding how the SML restratifies is particularly important to global climate models, which rely on accurate representations of sea surface temperature but approximate the SML at each grid point as being independent of horizontally adjacent points. The SML may exhibit a considerably more complicated structure, however, not only in the vertical [Sprintall and Roemmich, 1999] but also in the horizontal. The horizontal dimension is important to restratification processes that compete with mixing; examples being the slumping of horizontal density gradients [Brainerd and Gregg, 1993, 1997; Tandon and Garrett, 1994, 1995] arising from spatially nonuniform buoyancy fluxes,  $J_b$ , imposed at the sea surface and from interleaving [Gregg, 1976; May and Kelley, 2002]. Recent modelling

studies [Haine and Marshall, 1998; G. Boccaletti et al., Mixed layer instabilities and restratification, submitted to *Journal of Physical Oceanography*, 2006, hereinafter referred to as Boccaletti et al., submitted manuscript, 2006] suggests baroclinic instability within the SML at frontal regions introduces horizontal density gradients at scales  $O(1\text{ km})$  that restratify the SML on typical scales of 1 day and therefore constrain the effects of atmospheric forcing to a thin surface layer. Climate models do not currently resolve such small temporal and spatial scales and an accurate understanding of their role in modifying the SML is required to properly parameterize their effects.

[3] Previous observations considered the SML during mid-winter when vertical mixing was strong [Ferrari and Rudnick, 2000]. The SML, which they defined by the depth range within which density was within  $0.1\text{ kg m}^{-3}$  of the shallowest value, extended to  $\sim 150\text{ m}$  during their observations along  $140^{\circ}\text{W}$  between  $25$  and  $35^{\circ}\text{N}$ , January 24 to February 20 1997. Density compensation, which occurs when the effect on density of a horizontal temperature gradient is cancelled by a coincident salinity gradient, was evident at horizontal scales of  $10\text{ m}$ – $10\text{ km}$  despite the presence of significant thermohaline gradients. The degree of compensation is quantified by the horizontal density ratio,  $R_\rho = \alpha\Delta\theta/\beta\Delta S$ , where  $\alpha$  and  $\beta$  are the expansion coefficients of potential temperature,  $\theta$ , and salinity,  $S$ , and  $\Delta\theta$  and  $\Delta S$  are their differences over a horizontal distance. Compensation occurs when  $R_\rho = 1$ , excess thermal effects cause density gradients when  $R_\rho \geq 1$ , and salinity gradients dominate when  $0 \leq R_\rho \leq 1$ .

[4] Ferrari and Rudnick [2000] proposed that the limiting lengthscale of  $10\text{ km}$  corresponded to an internal Rossby radius,  $Ro_B = NH/f$ , where  $N = \sqrt{-\frac{g}{\rho_0} \frac{\Delta\rho}{\Delta z}}$  is the buoyancy frequency,  $H$  is the depth of the SML and  $f$  is the Coriolis frequency.  $Ro_B$  was computed using  $\Delta\rho$  across the SML base. At scales  $\leq Ro_B$ , horizontal density gradients are believed to slump under gravity and diffuse. At scales  $> Ro_B$ , horizontal density gradients exist in geostrophic balance. Rudnick and Martin [2002] find the tendency for compensation increases with mixed layer depth based on a survey of data collected over the past 15 years. Increasing evidence, however, points towards the importance of sub-mesoscale ( $\leq 10\text{ km}$ ) horizontal density gradients to the restratification processes that generate non-zero vertical density gradients within the SML when the atmospheric forcing is not strong enough to produce vertical mixing.

[5] Here we analyze observations from 3 March to 24 March 2004 between  $28$  and  $30^{\circ}\text{N}$ ,  $-150$  and  $-148^{\circ}\text{E}$ . The region includes the Subtropical Front (STF) in the north-east Pacific, as did Ferrari and Rudnick [2000], but meteorological conditions during our experiment were much

<sup>1</sup>Applied Physics Laboratory, University of Washington, Seattle, Washington, USA.

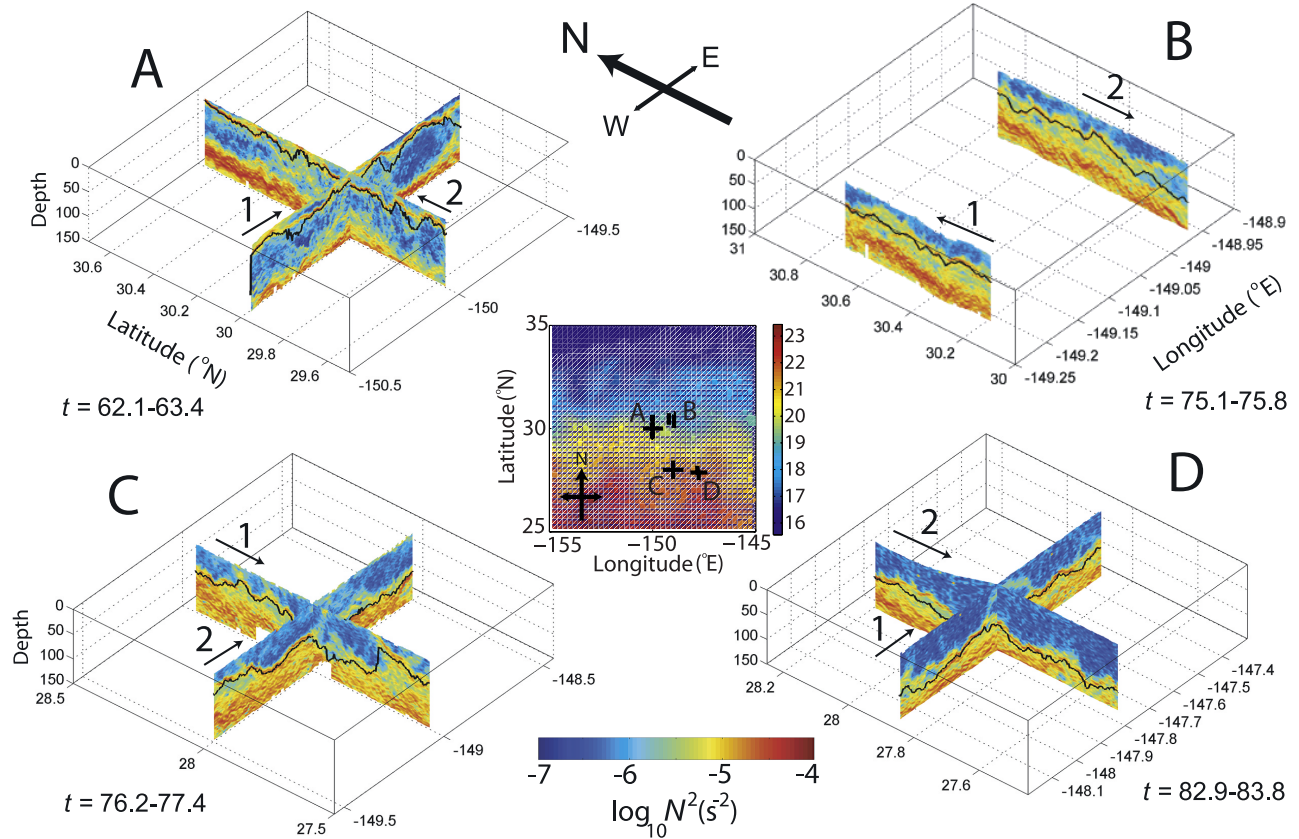


**Figure 1.** (middle) Location of surveys A, B, C, and D relative to the STF as indicated by the sea surface temperature (SST). (left and right) Buoyancy frequency squared,  $N^2$ , between 0 and 150 m depth for each survey, labelled accordingly. Solid black lines in the  $N^2$  plots indicate the depth of the SML according to the  $0.1 \text{ kg m}^{-3}$  density criteria (see text), and the numbered arrows indicate the order and direction of legs. Note the  $45^\circ$  anti-clockwise rotation of the  $N^2$  plots relative to the SST map. SST data are a three-day average for 5–7 March,  $t = 64$ –66, acquired by the TMI/AMSR satellite and provided by Remote Sensing Systems.

more variable. Using the Shallow Water Mapping System (SWIMS), an undulating CTD system towed behind the R/V *Wecoma* in a saw-tooth pattern between depths of 10–150 m with a mid-depth horizontal resolution of  $\leq 500$  m, horizontal variability in the density field and the degree of compensation above the seasonal thermocline was observed in four surveys at scales 1–25 km. Data were interpolated onto a uniform grid with 1 km spacing in the horizontal and 0.5 m in the vertical. Each survey, designated A, B, C, and D in chronological order, consisted of two 100 km legs, one north-south (N-S), the other east-west (E-W) with the exception of B which had two N-S legs only (Figure 1, center).

## 2. Meteorology

[6] Meteorological data were acquired onboard the R/V *Wecoma*, and Version 2.6 of the COARE bulk algorithms [Bradley et al., 2000] was used to compute the air-sea fluxes. Of principal interest to the mixing and restratification of the SML is the buoyancy flux,  $J_b$ , where positive  $J_b$  destabilizes the SML and negative values represent stabilizing, restratifying conditions. The dominant terms are  $Q_{\text{shortwave}}$  and  $Q_{\text{latent}}$ . The former stabilizes via solar insolation whereas the latter destabilizes during high winds.

[7] Total rainfall during the 25 days was 205 mm (Figure 2a) and concentrated within three events during

days 62, 67, and 78 when rainrate  $\geq 40 \text{ mm hr}^{-1}$  and accumulated rainfall  $\geq 25 \text{ mm}$ . Wind stress,  $\tau$ , peaked at 1.2 and  $0.7 \text{ N m}^{-2}$  during the latter two events (typically following the rainfall by up to 24 hours). Prior to A  $\tau$  remained  $\leq 0.25 \text{ N m}^{-2}$  when  $\Delta T = T_{\text{sea}} - T_{\text{air}} \leq 1^\circ\text{C}$  (Figure 2b) and  $J_b$  was largely negative, i.e., stabilizing (Figure 2c), particularly during the rainfall at  $t = 62.9$ . The two peaks in  $\tau$  were accompanied by cold air outbreaks resulting in  $\Delta T \geq 4^\circ\text{C}$  whilst a third period of lesser  $\tau \leq 0.25 \text{ N m}^{-2}$  on day 73 also exhibited significant  $\Delta T$  immediately prior to B. Note that during the transit from B at  $30^\circ\text{N}$  to C at  $28^\circ\text{N}$  the R/V *Wecoma* passed through a surface temperature front.  $T_{\text{sea}}$  increased from  $18.56^\circ\text{C}$  to  $22.06^\circ\text{C}$  within 25 km and  $\Delta T \geq 0$  for the remainder of the cruise despite a recovery of  $T_{\text{air}}$  to  $22.54^\circ\text{C}$  by  $t = 77.9$  after the second cold air outbreak. Thus prior to D,  $J_b$  was destabilizing during nighttime when latent heat fluxes were  $O(100 \text{ W m}^{-2})$ . A maximum  $J_b$  of  $3.2 \times 10^{-7} \text{ W kg}^{-1}$  was observed at the time of peak  $\tau$  on day 79, three days before D.

## 3. Vertical Structure of the SML

[8] In contrast to previous observations in which a well-mixed SML extended down to the seasonal thermocline, we observed significant vertical density structure above the

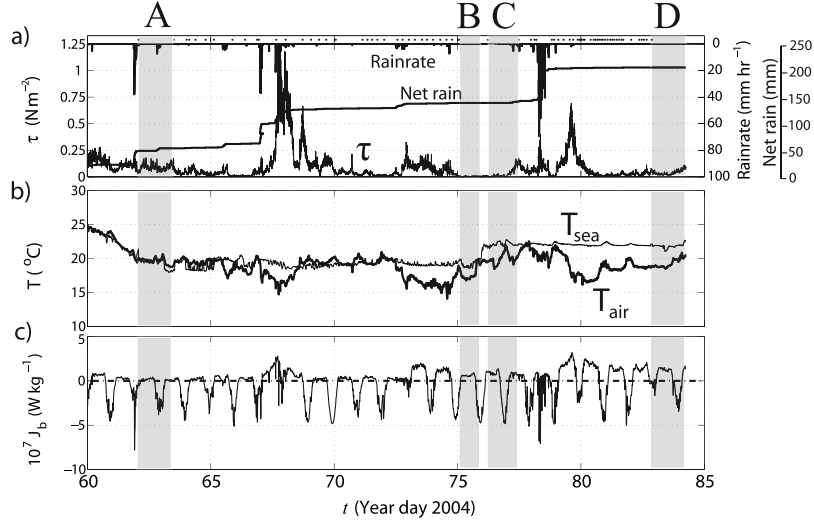


**Figure 2.** Meteorological data from the R/V *Wecoma*: (a) Wind stress ( $\tau$ ), rainrate, and net rain, (b) air and sea temperature, and (c) buoyancy flux ( $J_b$ ). The duration of the surveys are shaded grey and labelled accordingly. Dots along the top of Figure 2a indicate the beginning of each SWIMS group conducted throughout the experiment.

seasonal thermocline in all surveys except D (Figure 1, left and right), due partly to the particularly heavy rainfall during the winter of 2003/2004. The essential characteristics of each survey are:

[9] 1. During survey A a steady north-westerly wind of  $10 \text{ ms}^{-1}$  and  $\Delta T \leq 1^\circ\text{C}$ , a thin, highly stratified layer of thickness  $\leq 20 \text{ m}$  was observed at  $\sim 30 \text{ m}$  in which  $N^2 \geq 10^{-5} \text{ s}^{-2}$ . Based on the  $\Delta\rho = 0.1 \text{ kg m}^{-3}$  criterion (used throughout this paper for comparison with the work of Ferrari and Rudnick [2000]), the SML base was always  $\leq 40 \text{ m}$ . The seasonal thermocline slopes upwards to the north from  $150 \text{ m}$  at  $29.6^\circ\text{N}$  to  $\sim 120 \text{ m}$  at  $30.4^\circ\text{N}$ . A remnant layer in which  $N^2$  varied about  $10^{-6} \text{ s}^{-2}$  by an order of magnitude existed between the thermocline and the near surface stratification.

[10] 2. In survey B the remnant layer persisted beneath the base of the SML 12 days after A despite the storms on days 68 and 73. The SML, in which  $N^2 \leq 10^{-6} \text{ s}^{-2}$ , had deepened by  $20\text{--}40 \text{ m}$  relative to A but still remained some  $50 \text{ m}$  above the seasonal thermocline. Mixing due to the storms was not sufficient to eradicate the stratification observed within the SML during A.

[11] 3. In survey C the SML on the southern side of the temperature front, crossed during the transit to  $28^\circ\text{N}$ , fluctuated between  $40$  and  $110 \text{ m}$  during similar meteorological conditions to B (light wind, weakly destabilizing  $J_b$ ). Near-surface  $N^2$  fell to  $O(10^{-7})$  towards the end of leg 2 as winds increased to  $\geq 10 \text{ ms}^{-1}$  and the SML deepened to  $100 \text{ m}$ . In the center of the survey the SML extended to the top of the seasonal thermocline whilst strong near-surface  $N^2$  to the north, south and west edges of the survey produced remnant layers with  $10^{-6} \leq N^2 \leq 10^{-5} \text{ s}^{-2}$  between  $\sim 50$  and  $100 \text{ m}$ . Significant lateral density gradients were observed as steeply sloping isopycnals whose vertical component contributed to  $N^2$ .

[12] 4. In survey D active convection due to  $J_b \geq 2 \times 10^{-7} \text{ W kg}^{-1}$  penetrated throughout the entire SML, inhibiting the restratification of the recently mixed SML, within which  $N^2 \leq 10^{-6} \text{ s}^{-2}$ , except for a thin layer in leg 1 that

rose to  $\leq 30 \text{ m}$  during nighttime and was not due to the diurnal cycle. Overturning during nighttime extended to the top of the seasonal thermocline across which vertical turbulent entrainment was observed in a low gradient Richardson number environment ( $Ri \leq 0.5$ ) due to inertial shear resulting from the storm on day 79.

[13] Brainerd and Gregg [1995] show that the  $\Delta\sigma_\theta$  criteria used here to define the SML is inadequate when the mixed layer does not reach the seasonal thermocline, i.e., when the *mixing* and *mixed* layers do not coincide. They show that any definition requires tuning for local conditions but that, in the presence of variable stratification, overturning may be constrained above the depth where  $\Delta\sigma_\theta$  exceeds the surface value by  $\leq 0.05 \text{ kg m}^{-3}$ . We use the  $0.1 \text{ kg m}^{-3}$  definition here to compare with previous studies.

#### 4. Lateral Density Structure

[14] Wavelet coefficients [Torrence and Compo, 1998] of the temperature and salinity contributions to density were calculated as functions of position  $x_o$  and scale  $l$  as;

$$\Delta\psi(l, x_o) = \frac{1}{|l|} \int_{-\infty}^{\infty} g^*(x) \frac{(x - x_o)}{|l|} \psi(x) dx \quad (1)$$

where  $\Delta\psi$  is the horizontal gradient in potential temperature or salinity,  $g^*(x)$  is the complex conjugate of the Morlet wavelet,  $g(x) = e^{\frac{x^2}{2}} e^{iQx}$ , and  $Q$  is the quality factor =  $2\sqrt{2\pi}$ , chosen for consistency with Ferrari and Rudnick [2000]. The wavelet coefficients, after scaling with the appropriate expansion coefficient, thus give the density gradient attributable to thermal and saline effects over the chosen scale and were used to compute  $R_\rho$ . We chose scales of 2, 5 and 10 km.

[15] At  $30^\circ\text{N}$  (surveys A and B), there was a tendency towards compensation, particularly at B, despite contributions by both thermohaline components frequently reaching  $0.1 \text{ kg m}^{-3}$  (Figure 3). At A,  $R_\rho$  increases at small scales but the distribution of points at all scales is more scattered

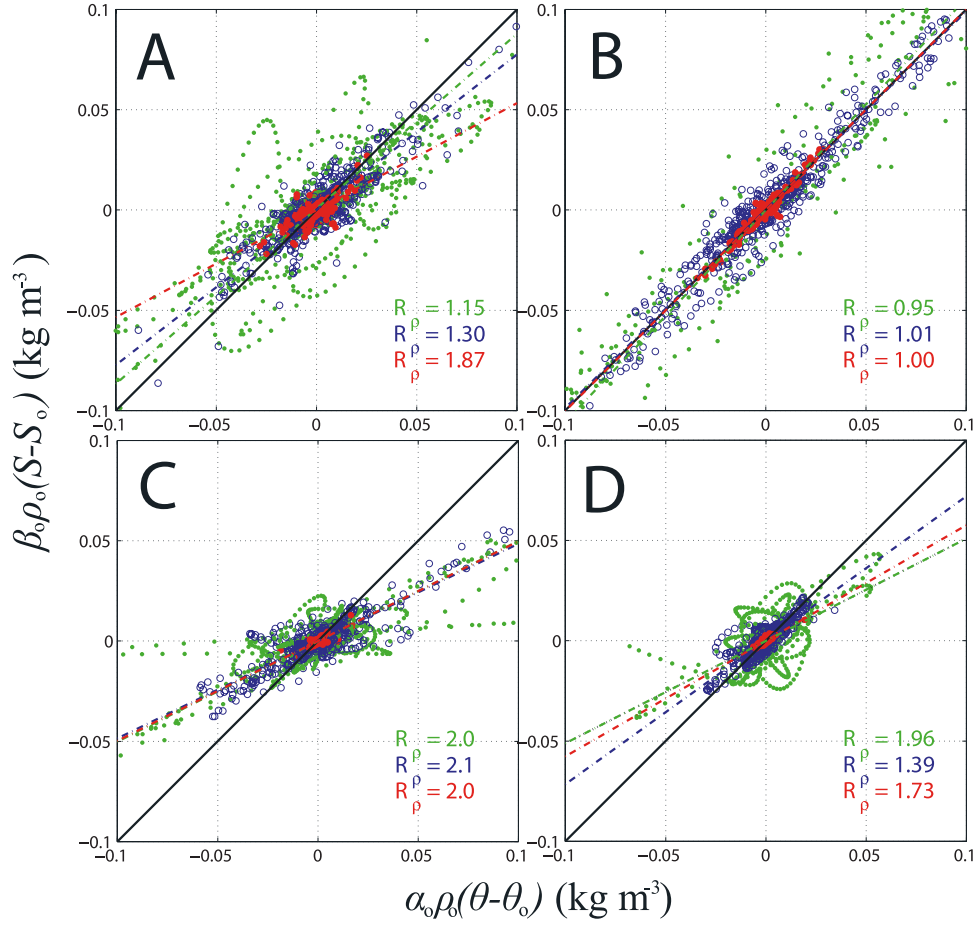


**Figure 3.** Scatterplots of the density-scaled wavelet coefficients of potential temperature (x-axis) against salinity (y-axis) along 20 m at 2 km (red), 5 km (blue), and 10 km (green) wavelengths for each survey (indicated in the top left corner of each panel). The solid black diagonal line corresponds to  $R_\rho = 1$ , i.e., density compensation. The least squares fit for each scale is indicated by the coloured dashed lines and the corresponding  $R_\rho$  stated in the lower right corner.

relative to B, where the largest thermohaline gradients were observed but were almost completely compensated. The greater scatter in A (i.e., departure from compensation) arises principally from the smaller uncompensated gradients in the E-W leg rather than the N-S leg in which thermohaline variance was  $\geq 0.05 \text{ kg m}^{-3}$  at 5 and 10 km wavelengths but largely compensated. Note that B, with two N-S legs, was conducted when wind stress was negligible and  $J_b$  was weak and destabilizing. Although the survey followed two strong storms, the SML was homogenous but did not extend to the seasonal thermocline.

[16] At 28°N (surveys C and D), there was a tendency to  $R_\rho = 2$  (i.e., temperature dominated) at all scales, particularly at C. The structure of the SML differed markedly between the two surveys. D followed vigorous mixing by the storm on day 79 and was representative of the well-mixed conditions observed by Ferrari and Rudnick [2000], whereas C was subjected to negligible wind stress but a destabilizing  $J_b$  after crossing the oceanic temperature front. As at A, thermohaline gradients in the N-S leg of C were  $\sim$  twice those in the E-W leg but, in contrast to A, the N-S leg exhibited the same lack of compensation as the E-W leg. The magnitude of thermohaline gradients at D are  $\sim$  half

those at C but retain the tendency to  $R_\rho = 2$  in the least squares fit.

[17] Further information on the density structure during specific sections may be obtained from the wavelet scalograms which indicate the magnitude of density gradients along an isobar as a function of scale and position. We consider the N-S sections at 20 m depth during C and D and compute  $Ro_{ML}$  using  $N$  within the SML and its depth. Density varied by  $\geq 0.25 \text{ kg m}^{-3}$  over 100 km at C and sharp gradients were clearly governed by temperature (Figure 4a). Variance equivalent to a gradient of  $0.001 \text{ kg m}^{-4}$  extended to horizontal scales of 2 km (Figure 4b, indicated by the blue contour), and, except at 55 km where the edge of a mesoscale eddy was crossed, matches  $Ro_{ML}$  to within a factor of 2. In contrast, during D which followed strong vertical mixing, density varied by  $\leq 0.125 \text{ kg m}^{-3}$  over the entire leg. Abrupt gradients were absent and density variance was constrained to scales  $\geq 5 \text{ km}$ . Due to the deeper SML and weak stratification,  $Ro_{ML} \sim 10 \text{ km}$  which was previously proposed as the limiting lengthscale during winter when forcing was strong. Spice,  $\tau \equiv \alpha \Delta \theta + \beta \Delta S$ , variance is  $\sim 10^2$  larger than density variance and exceeds noise

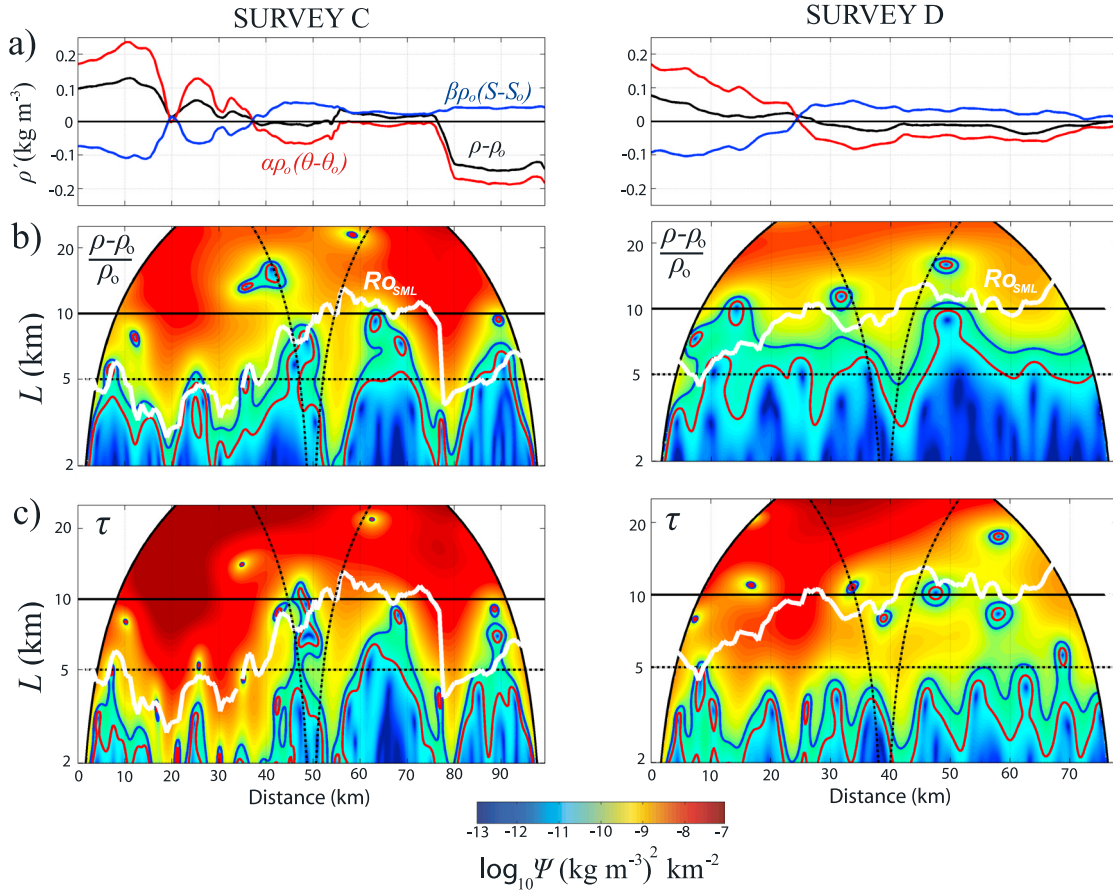


**Figure 4.** a) Horizontal sections at 20 m of temperature and salinity contributions to density perturbations and the resultant density during the N-S legs of surveys C and D, and the corresponding wavelet scalograms of (b) density,  $(\rho - \rho_0)/\rho_0$ , and (c) spice,  $\tau = \alpha(\theta - \theta_0) + \beta(S - S_0)$ . Dashed black lines in the center of each scalogram indicate the resolution at each wavelength,  $L$ . The blue and red contours correspond to gradients of  $0.01$  and  $0.005 \text{ kg m}^{-3}$ , respectively, at a  $10 \text{ km}$  wavelength. The white solid line is the localized internal Rossby radius,  $Ro_{ML}$ .

levels down to our lowest resolvable scale of  $2 \text{ km}$  (Figure 4c).

## 5. Summary and Discussion

[18] Our observations indicate a clear distinction between the regimes at  $28^\circ\text{N}$  and  $30^\circ\text{N}$ . There was a tendency for compensation to the north despite large thermohaline gradients of  $\geq 2^\circ\text{C}$  and  $0.6 \text{ ppt}$  over  $10 \text{ km}$ , whereas in the south uncompensated density fronts were dominated by temperature, evident as  $R_\rho \geq 1$ . The highly variable meteorological conditions undoubtedly had a strong influence on the vertical structure of the SML, particularly in forming shallow haloclines and remnant layers, but the large-scale distinction is due to the climatological structure of the STF. The position and thermohaline composition of the fronts are virtually the same as those presented by Roden [1980] and Samelson and Paulson [1988]. They observed 3 frontal regions in the STF, the southernmost of which at  $28^\circ\text{N}$  ( $27^\circ\text{N}$  in the work of Samelson and Paulson [1988]) was an uncompensated temperature front, whereas that at  $31^\circ\text{N}$  was compensated and represented the northern bound-

ary of North Pacific Central Water. Ferrari and Young [1997] propose that compensation at scales  $\leq 10 \text{ km}$  is achieved due to a dependence of the horizontal diffusivity on the lateral buoyancy gradient. Horizontal buoyancy gradients, arising from nonuniform surface forcing and large-scale stirring, are erased by vertical mixing as dense water slumps beneath light water. Such a mechanism may explain the tendency towards compensation at  $30^\circ\text{N}$  but not the temperature-dominated regime further south where  $R \geq 1$  at all scales. Stommel [1993] conjectures that a ‘mixed layer regulator’ model explains the observed basin-scale  $R_\rho = 2$  by asymmetries in the thermal and haline atmospheric forcing of the upper ocean. Ferrari and Rudnick [2000] suggest that  $R_\rho = 2$  may be achieved through this mechanism by strong localized fronts interspersing an otherwise compensated ocean. Our results would appear to support the latter interpretation, but a definitive explanation requires longer sections through the SML.

[19] The small scales to which lateral density variability extended in the vicinity of the front at  $28^\circ\text{N}$  are not directly related to the large scale dynamics, however, and are in

direct contrast to previous observations in which compensation was ubiquitous at scales  $\leq 10$  km. Spatial variability in surface fluxes, particularly penetrative solar radiation, does not account for the horizontal density variability. The majority of measurements were made during nighttime when winds were light and convection was weak with the exception of D where the SML was well-mixed.

[20] The presence of transient stratification above the seasonal thermocline in our observations introduces an additional dynamical mechanism for generating lateral density structure at scales  $\leq Ro_B$ . A modified mixed layer internal Rossby radius,  $Ro_{ML}$ , computed using  $\Delta\rho$  within the SML rather than across the base of the SML, is 2–5 km and varies strongly with position over short distances. This is the preferred lengthscale for mixed layer baroclinic instabilities, proposed by (Boccaletti et al., submitted manuscript, 2006) to be responsible for the restratification of the SML and lateral density gradients at lengthscales as small as 1 km.  $Ro_{ML}$  corresponds to within a factor 2, and generally less, of the lengthscale to which horizontal density variability is observed in our data and strongly suggests that baroclinic instability is the primary mechanism responsible for restratification of the SML. Strong vertical mixing eradicates the transient stratification so that the base of the SML coincides with the seasonal thermocline and  $Ro_{SML}$  tends towards scales commensurate with  $Ro_B$ . The greater variance in  $\tau$  at all scales is further indicative of the persistence of compensated thermohaline gradients that are not dissipated by the vertical mixing that erases density gradients (Boccaletti et al., submitted manuscript, 2006). Our observations suggest that, particularly near large-scale fronts, restratification occurs due to horizontal processes at scales not typically resolved in numerical models of the SML and thus needs to be properly parameterized if the models are to avoid overestimating the depth of the SML.

[21] **Acknowledgments.** This work was funded by the U.S. National Science Foundation under grant OCE0326280. We are indebted to Frank Bradley for setting up the rain gauges and providing their outputs. We thank Jack Miller, Eric Boget, Paul Aguilar, John Mickett, Avery Snyder, Glenn Carter, Dave Winkel, Steve Bayer, and Andrew Cookson for their help in collecting the data and the captain and crew of the R/V *We come* for their assistance during difficult conditions.

## References

- Bradley, E. F., C. W. Fairall, J. E. Hare, and A. A. Grachev (2000), An old and improved bulk algorithm for air-sea fluxes, paper presented at 14th Symposium on Boundary Layers and Turbulence, Am. Meteorol. Soc., Aspen, Colo.
- Brainerd, K. E., and M. C. Gregg (1993), Diurnal restratification and turbulence in the oceanic surface mixed layer: 1. Observations, *J. Geophys. Res.*, **98**, 22,645–22,656.
- Brainerd, K. E., and M. C. Gregg (1995), Surface mixed and mixing layer depths, *Deep Sea Res., Part I*, **42**, 1521–1543.
- Brainerd, K. E., and M. C. Gregg (1997), Turbulence and stratification on the Tropical Ocean-Global Atmosphere-Coupled Ocean-Atmosphere Response Experiment microstructure pilot cruise, *J. Geophys. Res.*, **102**, 10,437–10,455.
- Ferrari, R., and D. L. Rudnick (2000), Thermohaline variability in the upper ocean, *J. Geophys. Res.*, **105**, 16,857–16,883.
- Ferrari, R., and W. R. Young (1997), On the development of thermohaline correlations as a result of nonlinear diffusive parameterizations, *J. Mar. Res.*, **55**, 1069–1101.
- Gregg, M. C. (1976), Finestructure and microstructure observations during the passage of a mild storm, *J. Phys. Oceanogr.*, **6**, 528–555.
- Haine, T. W. N., and J. Marshall (1998), Gravitational, symmetric, and baroclinic instability of the ocean mixed layer, *J. Phys. Oceanogr.*, **28**, 634–658.
- May, B. D., and D. E. Kelley (2002), Contrasting the interleaving in two baroclinic ocean fronts, *Dyn. Atmos. Oceans*, **36**, 23–42.
- Roden, G. I. (1980), On the subtropical frontal zone north of Hawaii during winter, *J. Phys. Oceanogr.*, **10**, 342–362.
- Rudnick, D. L., and J. P. Martin (2002), On the horizontal density ratio in the upper ocean, *Dyn. Atmos. Oceans*, **36**, 3–21.
- Samelson, R. M., and C. A. Paulson (1988), Towed thermistor chain observations of fronts in the subtropical North Pacific, *J. Geophys. Res.*, **93**, 2237–2246.
- Sprintall, J., and D. Roemmich (1999), Characterizing the structure of the surface layer in the Pacific Ocean, *J. Geophys. Res.*, **104**, 23,297–23,311.
- Stommel, H. M. (1993), A conjectural mechanism for determining the thermohaline structure of the oceanic mixed layer, *J. Phys. Oceanogr.*, **23**, 142–158.
- Tandon, A., and C. Garrett (1994), Mixed layer restratification due to a horizontal density gradient, *J. Phys. Oceanogr.*, **24**, 1419–1424.
- Tandon, A., and C. Garrett (1995), Geostrophic adjustment and restratification of a mixed layer with horizontal gradients above a stratified layer, *J. Phys. Oceanogr.*, **25**, 2229–2241.
- Torrence, C., and G. P. Compo (1998), A practical guide to wavelet analysis, *Bull. Am. Meterol. Soc.*, **79**, 61–78.

---

M. H. Alford, M. C. Gregg, and P. Hosegood, Applied Physics Laboratory, University of Washington, 1013 NE 40th Street, Seattle, WA 98105-6698, USA. (hosegood@apl.washington.edu)